Tailored silver nanoparticle arrays for enhanced polarization-anisotropic second-harmonic emission

Lingrui Chu,[1] Rang Li,[2] Han Zhu,[1] Weijie Liu,[1] Hiroshi Amekura,[3] Norito Ishikawa,[4] Nariaki Okubo,[4] Xiaoli Sun,[1,a)] and Feng Chen[1,a)]

[1]*School of Physics, State Key Laboratory of Crystal Materials, Shandong University, Jinan 250100, China*

[2]*Institute of Ion Beam Physics and Materials Research, Helmholtz-Zentrum Dresden-Rossendorf, Dresden 01328, Germany*

[3]*National Institute for Materials Science (NIMS), Tsukuba 305-0003, Japan*

[4]*Japan Atomic Energy Agency, Tokai 319-1195, Japan*

Nonlinear optical phenomena with polarization-dependent characteristics are pivotal for the advancement of integrated photonic devices. We present the remarkable second-harmonic generation (SHG) with pronounced polarization anisotropy, achieved through meticulously engineered silver (Ag) nanoparticle (NP) arrays. The spherical Ag NP arrays are initially fabricated beneath the surface of SiO_2 substrates via 160 keV Ag^+ ions implantation. Following this, the swift heavy-ion irradiation (SHII) at an energy of 200 MeV is applied to irradiate the embedded spherical Ag NPs in SiO_2 at a 45 degree angle relative to the surface normal. Under SHII, the Ag NPs are elongated along the Xe^{14+} ions trajectory and form rod-like structures with a uniform orientation across centimeter-scale areas, leading to the varied interparticle distances along the *x*- and *y*-directions. As a consequence, the engineered Ag NP arrays exhibit polarization-sensitive plasmonic optical responses across both the visible and near-infrared spectra, demonstrating a distinct dipole-like, polarization-dependent SHG response with an impressive anisotropy ratio of up to 25 (SHG intensity maxima under *x*-polarized laser excitations and minima under *y*-polarized laser excitations). Notably, the SHG intensity from the tailored Ag NP arrays is comparable to that of two-dimensional transition metal dichalcogenides. The unique polarization-dependent nonlinearity offered by these extensive Ag NP arrays presents significant potential for integrated nonlinear photonic applications that harness polarization functionality.

Nonlinear optics plays a vital role in modern science and technology, with applications ranging from materials analysis to quantum information processing.[1-4] Recently, second-order nonlinear processes, particularly second-harmonic generation (SHG), have garnered considerable attention in nanostructured materials due to their potential in integrated nonlinear optical applications.[5-7] SHG occurs at the surfaces of nanostructures where inversion symmetry is broken and is greatly amplified by the localized surface plasmon resonance (LSPR)-induced electric field enhancements at both fundamental and second-harmonic wavelengths.[5, 6]

Intensive research has focused on boosting second-order nonlinearities in plasmonic nanostructures that confine light to nanoscale volumes. For instance, intense SHG has been demonstrated in plasmonic nano-cavities,[5, 6, 8, 9] which

[a)]Author to whom correspondence should be addressed. Electronic mail: xlsun@sdu.edu.cn (Xiaoli Sun), drfchen@sdu.edu.cn (Feng Chen)

hold great potential for the development of nonlinear nanophotonic devices, including nanoscale light sources and ultrafast integrated all-optical switches. However, conventional synthesis techniques, such as chemical techniques[5] and electron beam lithography,[10, 11] often struggle to achieve uniformly distributed and densely packed plasmonic nanocavities or nanodimers with polarization-dependent optical responses over large areas. In the uniformly distributed plasmonic nanostructures, the LSPR response could be dynamically tuned by varying the polarization of the incident light, enabling distinct nonlinear optical processes such as frequency conversion and nonlinear absorption with unusual polarization properties.[12-14] This capability expands the utility of integrated nonlinear optical components, paving the way for advanced photonic devices that manipulate light in ways dependent on its polarization state. Achieving large-scale plasmonic nanostructures with both consistent orientations and nanoscale light confinement presents significant opportunities for advancing nonlinear nanophotonics with polarization functionality. Recently, ion implantation has emerged as a simple and cost-effective method for fabricating embedded nanoparticles (NPs) beneath a substrate's surface in a large area.[15-18] Meanwhile, the swift heavy-ion irradiation (SHII) can elongate the metallic NPs into rod-like shapes over large areas, facilitating the effective production of large-scale, uniformly oriented plasmonic nanostructures.[19-21] By controlling the incident light polarizations, the plasmonic response can be tailored, enhancing its applicability in nonlinear optical processes with polarization functions.

In this work, we demonstrate the second-harmonic emission with exceptional polarization anisotropy in the large-area tailored Ag NP arrays. The elongated Ag NPs, aligned uniformly over a centimeter-scale area, are fabricated beneath a SiO_2 substrate via Ag^+ ion implantation followed by swift heavy-ion (200 MeV Xe^{14+}) irradiation. Both strong second-order nonlinearity and exceptional optical anisotropy are simultaneously achieved in the elongated Ag NP arrays. The Xe^{14+} ion irradiation aligns the elongated Ag NPs in a uniform orientation, resulting in a remarkable polarization anisotropy in SHG, where the polarization anisotropy ratio reaches up to 25 under the excitation of a fundamental wave at 1064 nm. Meanwhile, the densely packed Ag NPs creates nanocavities with significantly enhanced electric fields at the nanoscale volume between adjacent elongated Ag NPs, leading to SHG intensity comparable to that of WS_2 monolayer. The large-area, tailored Ag NP arrays exhibiting polarization-dependent SHG could pave the way for integrated nonlinear nanophotonics with advanced polarization functions.

In the experiment, the embedded spherical Ag NPs are initially fabricated through direct low-energy ion implantation. The Ag^+ ions are implanted into SiO_2 substrate surfaces (10×10 mm^2) using an ion-implanter (LC22-1C0-01) with an energy of 160 keV to a fluence of 1×10^{17} ions/cm^2. During the implantation, discrete Ag ions would spontaneously aggregate into the crystalline Ag NPs after the nucleation, growth, and Ostwald ripening processes[17]. Figs. 1(a)-(b) present cross-sectional high-resolution transmission electron microscopy (HRTEM, Talos F200XG2)

images of spherical Ag NPs embedded within a SiO_2 substrate. The Ag NPs are distributed approximately 60 nm beneath the SiO_2 surface and have a diameter of around 40 nm. The high-angle annular dark field (HAADF) image and the corresponding Ag element mapping confirm the formation of spherical Ag NPs (Fig. 1(c)).

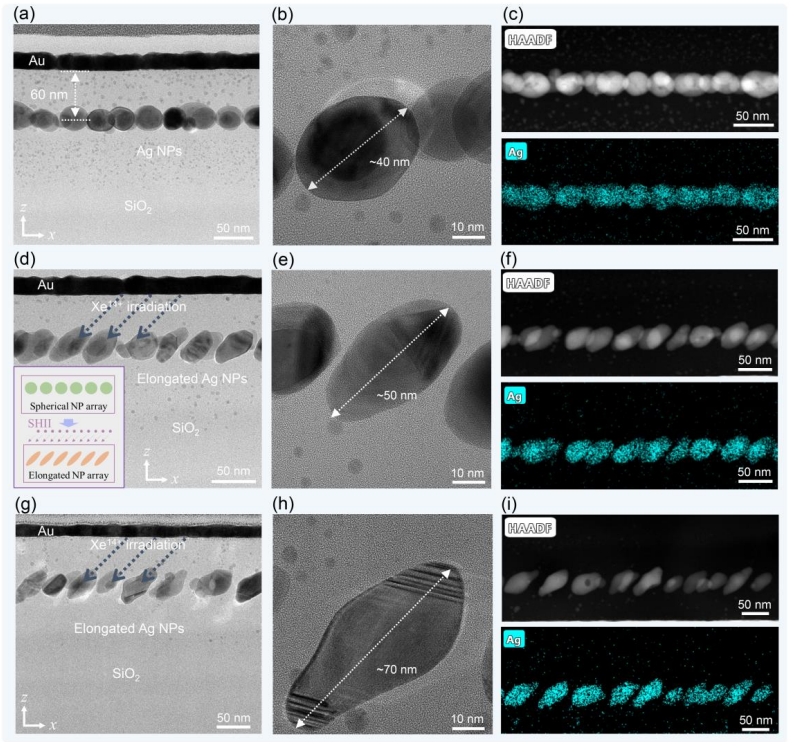

Figure 1. (a)-(b) Cross-sectional HRTEM images of spherical Ag NPs embedded in SiO_2 substrate. (c) HAADF image of the spherical Ag NPs, accompanied by the corresponding Ag element mapping. (d)-(e) Cross-sectional HRTEM images of elongated Ag NPs formed after Xe^{14+} irradiation at a fluence of 5×10^{13} ions/cm². The inset in (d) shows a diagram illustrating the formation of the elongated Ag NP arrays under SHII. (f) HAADF image of the elongated Ag NPs (Xe^{14+} ion irradiation fluence: 5×10^{13} ions/cm²) with corresponding Ag element mapping. (g)-(h) Cross-sectional HRTEM images of elongated Ag NPs fabricated through Xe^{14+} ion irradiation at a fluence of 1×10^{14} ions/cm². (i) HAADF image of the elongated Ag NPs with corresponding Ag element mapping.

The Ag-implanted SiO_2 samples were irradiated with swift heavy ions, specifically 200 MeV $^{136}Xe^{14+}$ ions, utilizing the 20 MV tandem accelerator at the Tokai Research and Development Center, JAEA. All the samples were irradiated at an incident angle of 45° from the surface normal, in order to elongate all the NPs in the *x*–*z* plane along a direction tilted 45° relative to the *x*-axis. Two distinct fluences were employed during the SHII process: 5×10^{13} and 1×10^{14} ions/cm². Upon exposure to SHII, the spherical Ag NPs undergo elongation, transforming into rod-like nanostructures. This method is well-established for the precise control of the shape and orientation of embedded

plasmonic NPs, a critical factor for their applications in photonics.[19-23] The elongation of the metallic particles results from the formation of molten ion tracks within the amorphous SiO_2 matrix.[19, 20] During irradiation, energy is deposited along the ion's trajectory as it interacts with the electrons in the matrix, leading to energy dissipation within a narrow cylindrical region surrounding the ion's path. As the lattice temperature exceeds the melting point of the material due to inelastic collisions, the regions along the ion's path become molten, resulting in an ion track upon cooling.[19, 24] Previous studies have demonstrated that spherical metallic NPs of more than ten metal species, including those made of gold (Au), silver (Ag), and platinum (Pt), embedded in SiO_2 can be reshaped into rod-like forms using this technique.[19-21, 25]

As shown in Figs. 1(d)-(e), the embedded Ag NPs are transformed into elongated, rod-like shapes following the SHII process. The elongated NPs have a major axis (d_{major}) of approximately 50 nm (Xe^{14+} irradiation fluence: 5×10^{13} ions/cm^2), which is significantly larger than the diameters of the original spherical Ag NPs. As indicated by the HRTEM images, the elongated Ag NPs exhibit excellent crystallinity. The inset of Fig. 1(d) provides an illustrative diagram depicting the formation of the elongated Ag NP arrays under the SHII process. Additionally, the HAADF image and Ag element mapping further demonstrate the elongation of the Ag NPs (Fig. 1(f)). To introduce a greater morphological anisotropy, the Xe^{14+} ion irradiation fluence is further increased to 1×10^{14} ions/cm^2. As a result, the elongation of Ag NPs becomes more pronounced, with the d_{major} reaching approximately 70 nm (Fig. 1(i)). In this case, the Ag NPs are elongated while remaining densely packed, maintaining strong interparticle coupling between neighboring NPs.

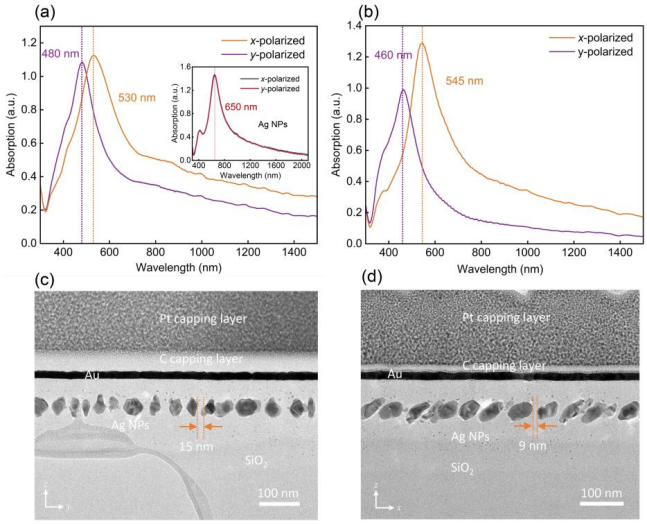

Figure 2. (a) Absorption spectra of the elongated Ag NPs (Xe^{14+} irradiation fluence: 5×10^{13} ions/cm^2) under *x*- and *y*-polarized light

illumination. Inset is the absorption spectra of embedded spherical Ag NPs under different polarized light illumination. (b) Absorption spectra of the elongated Ag NPs (Xe^{14+} irradiation fluence: 1×10^{14} ions/cm^2) under the *x*-polarized and *y*-polarized light illumination. (c) and (d) are cross-sectional HRTEM images of the elongated Ag NPs obtained from *y*-*z* and *x*-*z* planes, respectively.

To investigate the polarization-dependent plasmonic optical response of the elongated Ag NPs, the polarization absorption spectra are measured using a UV-Visible-NIR microspectrophotometer (20/30 PV, CRAIC Technologies) in the wavelength of 300 nm to 1500 nm, with a spectral sampling area of approximately 25 μm^2. As shown in Figs. 2(a) and (b), the elongated Ag NP arrays display distinct LSPR-induced optical absorption with polarization dependence in the visible and near-infrared bands. For the elongated Ag NPs irradiated with Xe^{14+} ions at a fluence of 5×10^{13} ions/cm², significant absorption differences are observed in elongated Ag NPs under *x*-polarized and y-polarized light illumination, with absorption peaks appearing at approximately 480 nm under *x*-polarized light illumination and 530 nm for *y*-polarized light illumination (Fig. 2(a)). In contrast, the spherical embedded Ag NPs show no difference in absorption under different polarized light illumination (inset of Fig. 2(a)). Furthermore, as the Xe^{14+} irradiation fluence increases to 1×10^{14} ions/cm², the elongated Ag NPs exhibit a higher optical polarization anisotropy, with a more pronounced absorption difference in the absorption spectra under different polarized light illuminations (Fig. 2(b)). Meanwhile, the elongated Ag NP arrays exhibit good reproducibility and scalability under the SHII process, with consistent optical absorption characteristics observed over a relatively large area (Fig. S1).

The polarization-dependent plasmonic optical response of the elongated Ag NPs in visible and near-infrared regions is primarily influenced by the varying sizes of nano-cavities along *x*- and *y*- directions. Although the NPs are elongated, they remain densely packed, with nano-cavities still existing between the neighboring NPs. When the orientation of elongated Ag NPs lies in the *x*-*z* plane, the sizes of nanocavities in *x*-direction and *y*-direction differ from each other. Figs. 2(c)-(d) are cross-sectional HRTEM images of the elongated Ag NPs (Xe^{14+} irradiation fluence: 1×10^{14} ions/cm^2) obtained from *y*-*z* and *x*-*z* planes, respectively. We observe that the distance between the elongated Ag NPs along the *y*-direction (mostly>10 nm) is significantly greater than the interparticle distance along the *x*-direction (generally<10 nm). In this case, the optical response will be different under light illuminations with varying

polarizations (Fig. S2). For the Ag plasmonic nanocavities, the LSPR-induced absorption peak occurs a wavelength blueshift as the size of the nanocavities increases.[15, 26, 27] As a result, the elongated Ag NP arrays exhibit a polarization-dependent optical response in the visible and near-infrared regions.

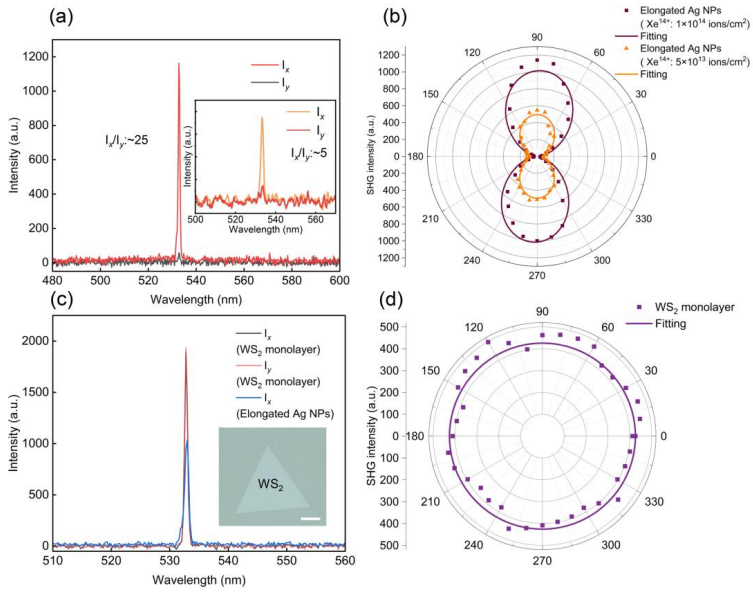

Figure 3. (a) SHG spectra of the elongated Ag NP arrays (Xe^{14+} irradiation fluence: 1×10^{14} ions/cm^2) excited under *x*- and *y*-polarized laser. Inset is the SHG spectra of the elongated Ag NP arrays (Xe^{14+} irradiation fluence: 5×10^{13} ions/cm^2). (b) Measured SHG intensity as a function of incident laser polarization. The polarization angle is fixed at 0 degree along the *y*-direction. (c) SHG spectra of the monolayer WS_2 and the elongated Ag NP arrays under the same measurement condition. Inset is the optical microscopy image of the WS_2 monolayer, and scale bar is 10 μm. (d) Measured polarization-dependent SHG intensity of monolayer WS_2.

The polarization-dependent nonlinear optical response of the elongated Ag NPs is investigated through the SHG measurements. A 1064-nm pulsed laser with a pulse width of ~20 ps and a repetition rate of 80 MHz is transmitted through a linear polarizer and a half-wave plate to excite the second-harmonic emission of the sample surface at 532 nm. The pump laser is tightly focused onto the sample surface with normal incidence using a 100× objective lens. The back-reflected second-harmonic emission is collected with the same objective lens and analyzed with a CCD camera. For the polarization-dependent SHG measurement, the half-wave plate is employed in the incident optical path to dynamically control the polarization of the incident laser, while no analyzer is applied in the collection optical

path.

As depicted in Fig. 3(a), the SHG spectra of elongated Ag NPs are obtained under *x*-polarized and *y*-polarized laser excitations with the same input power, respectively. A significant difference in SHG is observed, with an extraordinary anisotropy ratio (ρ) of ~25 in the elongated Ag NPs (subjected to Xe^{14+} irradiation at a fluence of 1×10^{14} ions/cm^2). Here, the polarization anisotropy is defined as $\rho = \frac{I_x}{I_y}$, with I_x and I_y referring the SHG intensities under *x*- and *y*-polarized laser excitations, respectively. For elongated Ag NPs subjected to Xe^{14+} ion irradiation at a lower fluence (5×10^{13} ions/cm²), the anisotropy ratio is relatively low, around ~5 (inset of Fig. 3(a)), suggesting that the elongation effect mainly contributes to SHG polarization anisotropy. In contrast, spherical Ag NPs show no SHG polarization anisotropy, showing comparable second-harmonic emission under both *x*- and *y*-polarized laser excitations (Fig. S3). To further investigate the polarization-dependent second-harmonic emission in elongated Ag NP arrays, polarization-dependent SHG spectra is measured. As shown in Fig. 3(b), the SHG intensity varies with incident laser polarization, displaying a double-lobed pattern with a maximum at 90° (*x*-direction) and a minimum at 0° (*y*-direction).

The SHG intensity of plasmonic nanostructures is strongly influenced by the local electric field enhancements at both the fundamental and second-harmonic (SH) frequencies. The SHG intensity ($I_{2\omega}$) could be approximately estimated as $I_{2\omega} \propto |f(\omega)|^4 \cdot |f(2\omega)|^2$,[28] where $f(\omega)$ and $f(2\omega)$ denotes the local field enhancement factors at the fundamental and SH frequencies, respectively. For the elongated Ag NP arrays, the SH wavelength (532 nm) is closer to the LSPR peak, a stronger near-field enhancement at SH frequency is achieved under *x*-polarized laser excitation. Additionally, the NPs are more closely packed along the *x*-direction, leading to a smaller interparticle gap and thus stronger coupling effects. This denser arrangement in the *x*-direction results in a broader red-shifted absorption band and enhanced local field strength at fundamental wavelength (1064 nm). Consequently, *x*-polarized laser excitation produces stronger near-field enhancements compared with *y*-polarized laser excitation at both fundamental and SH

wavelengths, ultimately giving rise to SHG anisotropy in the tailored Ag NP arrays.

To evaluate the SHG performance of the elongated Ag NPs, a WS_2 monolayer is utilized as a reference due to its significant second-order nonlinearity arising from broken inversion symmetry.[29] The WS_2 monolayers are synthesized via chemical vapor deposition (CVD), obtained from SixCarbon Technology, Shenzhen. As indicated in Fig. 3(c), the SHG intensity of the elongated Ag NPs is comparable to that of the WS_2 monolayer under *x*-polarized laser excitation, using identical measurement conditions: an input power of approximately 2.3 mW and an integration time of 4 seconds. The intense signal is attributed to significantly enhanced SHG at the surface of the Ag NPs, driven by strong local electric field amplification at both the fundamental and SH wavelengths.[16] While the WS_2 monolayer exhibits intense second-harmonic emission, it shows no polarization-dependent behavior (Fig. 3(d)). Common 2D materials like MoS_2,[30-33] WS_2,[29, 34],and WSe_2[35] typically exhibit strong second-order nonlinearity, but they do not simultaneously display strong nonlinearity and significant optical anisotropy.[36] In contrast, the fabricated elongated Ag NPs demonstrate both intense SHG and remarkable polarization anisotropy of up to 25, underscoring their potential for applications in nonlinear nanophotonics with advanced polarization functions.

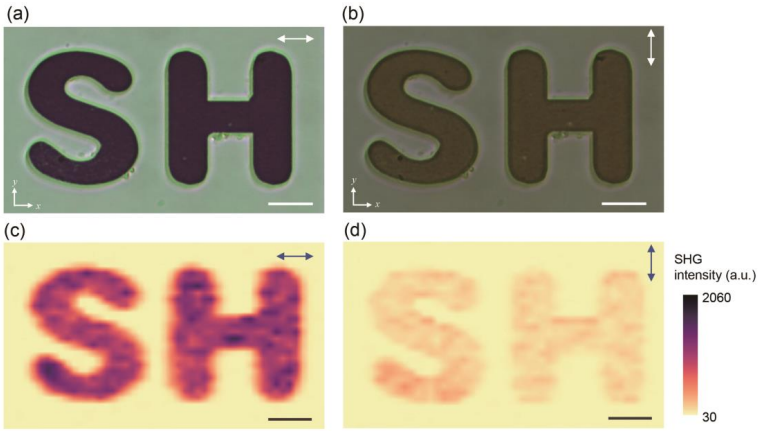

Figure 4. (a) and (b) are optical microscopy images of the elongated Ag NPs etched in "S" and "H" patterns under *x*- and *y*-polarized light illuminations, respectively. The etched depth is approximately 300 nm, which is significantly greater than the distribution depth of the Ag NPs. Scale bars: 10 μm. (c) and (d) are SHG mappings of the sample excited by *x*-and *y*-polarized 1064 nm pulsed laser, respectively. The SHG mappings are with a same color bar. Scale bars are 10 μm. The arrows denote the incident light polarization.

Next, polarization-dependent SHG mapping measurements are performed to intuitively illustrate the SHG polarization anisotropy. The elongated Ag NPs, subjected to Xe^{14+} irradiation fluence of 1×10^{14} ions/cm², are patterned into "S" and "H" shapes using focused ion beam (FIB) milling. Optical microscopy images of these patterns, illuminated with *x*- and *y*-polarized white light, exhibit distinct colors, indicating the polarization-dependent plasmonic optical response of the elongated Ag NPs. A noticeable difference in the intensity of second-harmonic emission is observed under *x*- and *y*-polarized laser excitation, as evidenced by the comparisons between Fig. 4(c) and Fig. 4(d), further certifying the intense second-harmonic emission with extraordinary polarization anisotropy. The nonlinear optical response with exceptional polarization anisotropy in tailored Ag NPs could also be extended to the other second-order and third-order optical processes with polarization functions, such as spontaneous photon down conversion (SPDC),[37] saturable absorption.[15]

In conclusion, intense second-harmonic emission with extraordinary polarization anisotropy is demonstrated in the elongated Ag NP arrays. The embedded Ag NPs are elongated with the same orientation across a large area via 200 MeV Xe^{14+} ion irradiation, resulting a significant polarization anisotropy in linear and nonlinear optical responses. Notably, the SHG of elongated Ag NP arrays is with a polarization anisotropy ratio of up to 25, comparable to that of monolayer WS_2 under the excitation of fundamental wave at 1064 nm. The achievement of robust nonlinear optical anisotropy alongside considerable optical nonlinearity in elongated, large-area Ag NP arrays opens exciting possibilities for the development of next-generation integrated photonic devices equipped with polarization functions.

SUPPLEMENTARY MATERIAL

See the supplementary material for more characterizations and simulation details.

DATA AVAILABILITY

The data that support the findings of this study are available from the corresponding author upon reasonable request.

ACKNOWLEDGMENTS

This work is supported by National Natural Science Foundation of China (Grant No. 12235009) and Taishan

Scholars Program of Shandong Province (No. tspd20210303). X. L. Sun acknowledges the support from "Young Scholars Program" and "Qilu Young Scholar Program" of Shandong University, China. The authors extend their gratitude to the Core Facility Sharing Platform of Shandong University. H.A. was supported by JSPS-KAKENHI Grant number 22K04990.

REFERENCES

[1]Y. R. Shen, "Surface properties probed by second-harmonic and sum-frequency generation," *Nature* **337**, 519-525 (1989).
[2]Y. Wang, J. Xiao, H. Zhu, Y. Li, Y. Alsaid, K. Y. Fong, Y. Zhou, S. Wang, W. Shi, Y. Wang, A. Zettl, E. J. Reed, X. Zhang, "Structural phase transition in monolayer $MoTe_2$ driven by electrostatic doping," *Nature* **550**, 487-491 (2017).
[3]J. L. O'Brien, "Optical Quantum Computing," *Science* **318**, 1567-1570 (2007).
[4]K.-Q. Lin, S. Bange, J. M. Lupton, "Quantum interference in second-harmonic generation from monolayer WSe_2," *Nat. Phys.* **15**, 242-246 (2019).
[5]G.-C. Li, D. Lei, M. Qiu, W. Jin, S. Lan, A. V. Zayats, "Light-induced symmetry breaking for enhancing second-harmonic generation from an ultrathin plasmonic nanocavity," *Nat. Commun.* **12**, 4326 (2021).
[6]M. Celebrano, X. Wu, M. Baselli, S. Großmann, P. Biagioni, A. Locatelli, C. De Angelis, G. Cerullo, R. Osellame, B. Hecht, L. Duò, F. Ciccacci, M. Finazzi, "Mode matching in multiresonant plasmonic nanoantennas for enhanced second harmonic generation," *Nat. Nanotechnol.* **10**, 412-417 (2015).
[7]R. Czaplicki, H. Husu, R. Siikanen, J. Mäkitalo, M. Kauranen, J. Laukkanen, J. Lehtolahti, M. Kuittinen, "Enhancement of Second-Harmonic Generation from Metal Nanoparticles by Passive Elements," *Phys. Rev. Lett.* **110**, 093902 (2013).
[8]X.-X. Wu, W.-Y. Jiang, X.-F. Wang, L.-Y. Zhao, J. Shi, S. Zhang, X. Sui, Z.-X. Chen, W.-N. Du, J.-W. Shi, Q. Liu, Q. Zhang, Y. Zhang, X.-F. Liu, "Inch-Scale Ball-in-Bowl Plasmonic Nanostructure Arrays for Polarization-Independent Second-Harmonic Generation," *ACS Nano* **15**, 1291-1300 (2021).
[9]Y. Zeng, H. Qian, M. J. Rozin, Z. Liu, A. R. Tao, "Enhanced Second Harmonic Generation in Double-Resonance Colloidal Metasurfaces," *Adv. Funct. Mater.* **28**, 1803019 (2018).
[10]B. K. Canfield, H. Husu, J. Laukkanen, B. Bai, M. Kuittinen, J. Turunen, M. Kauranen, "Local Field Asymmetry Drives Second-Harmonic Generation in Noncentrosymmetric Nanodimers," *Nano Lett.* **7**, 1251-1255 (2007).
[11]H. Aouani, M. Navarro-Cia, M. Rahmani, T. P. H. Sidiropoulos, M. Hong, R. F. Oulton, S. A. Maier, "Multiresonant Broadband Optical Antennas As Efficient Tunable Nanosources of Second Harmonic Light," *Nano Lett.* **12**, 4997-5002 (2012).
[12]A. E. Minovich, A. E. Miroshnichenko, A. Y. Bykov, T. V. Murzina, D. N. Neshev, Y. S. Kivshar, "Functional and nonlinear optical metasurfaces," *Laser Photon. Rev.* **9**, 195-213 (2015).
[13]J. Wang, A. Coillet, O. Demichel, Z. Wang, D. Rego, A. Bouhelier, P. Grelu, B. Cluzel, "Saturable plasmonic metasurfaces for laser mode locking," *Light-Sci. Appl.* **9**, 50 (2020).
[14]M. Kauranen, A. V. Zayats, "Nonlinear plasmonics," *Nat. Photonics* **6**, 737-748 (2012).
[15]R. Li, C. Pang, Z. Li, M. Yang, H. Amekura, N. Dong, J. Wang, F. Ren, Q. Wu, F. Chen, "Fused Silica with Embedded 2D-Like Ag Nanoparticle Monolayer: Tunable Saturable Absorbers by Interparticle Spacing Manipulation," *Laser Photon. Rev.* **14**, 1900302 (2020).
[16]L. Chu, Z. Li, H. Zhu, F. Ren, F. Chen, "Second-harmonic generation of embedded plasmonic nanoparticle arrays via interparticle coupling," *Appl. Phys. Lett.* **120**, 073104 (2022).
[17]R. Li, C. Pang, Z. Li, F. Chen, "Plasmonic Nanoparticles in Dielectrics Synthesized by Ion Beams: Optical Properties and Photonic Applications," *Adv. Opt. Mater.* **8**, 1902087 (2020).
[18]R. H. Magruder, L. Yang, R. F. Haglund, C. W. White, L. Yang, R. Dorsinville, R. R. Alfano, "Optical properties of gold nanocluster composites formed by deep ion implantation in silica," *Appl. Phys. Lett.* **62**, 1730-1732 (1993).
[19]M. C. Ridgway, R. Giulian, D. J. Sprouster, P. Kluth, L. L. Araujo, D. J. Llewellyn, A. P. Byrne, F. Kremer, P. F. P. Fichtner,

G. Rizza, H. Amekura, M. Toulemonde, "Role of Thermodynamics in the Shape Transformation of Embedded Metal Nanoparticles Induced by Swift Heavy-Ion Irradiation," *Phys. Rev. Lett.* **106**, 095505 (2011).

[20]P. Kluth, R. Giulian, D. J. Sprouster, C. S. Schnohr, A. P. Byrne, D. J. Cookson, M. C. Ridgway, "Energy dependent saturation width of swift heavy ion shaped embedded Au nanoparticles," *Appl. Phys. Lett.* **94**, 113107 (2009).

[21]K. Awazu, X. M. Wang, M. Fujimaki, J. Tominaga, H. Aiba, Y. Ohki, T. Komatsubara, "Elongation of gold nanoparticles in silica glass by irradiation with swift heavy ions," *Phys. Rev. B* **78**, 054102 (2008).

[22]Y. K. Mishra, F. Singh, D. K. Avasthi, J. C. Pivin, D. Malinovska, E. Pippel, "Synthesis of elongated Au nanoparticles in silica matrix by ion irradiation," *Appl. Phys. Lett.* **91**, 063103 (2007).

[23]R. Giulian, P. Kluth, L. L. Araujo, D. J. Sprouster, A. P. Byrne, D. J. Cookson, M. C. Ridgway, "Shape transformation of Pt nanoparticles induced by swift heavy-ion irradiation," *Phys. Rev. B* **78**, 125413 (2008).

[24]M. Toulemonde, C. Dufour, E. Paumier, "Transient thermal process after a high-energy heavy-ion irradiation of amorphous metals and semiconductors," *Phys. Rev. B* **46**, 14362-14369 (1992).

[25]R. Giulian, F. Kremer, L. L. Araujo, D. J. Sprouster, P. Kluth, P. F. P. Fichtner, A. P. Byrne, M. C. Ridgway, "Shape transformation of Sn nanocrystals induced by swift heavy-ion irradiation and the necessity of a molten ion track," *Phys. Rev. B* **82**, 113410 (2010).

[26]Z. Liu, H. Wang, H. Li, X. Wang, "Red shift of plasmon resonance frequency due to the interacting Ag nanoparticles embedded in single crystal SiO_2 by implantation," *Appl. Phys. Lett.* **72**, 1823-1825 (1998).

[27]T. Yamada, K. Fukuda, S. Semboshi, Y. Saitoh, H. Amekura, A. Iwase, F. Hori, "Control of optical absorption of silica glass by Ag ion implantation and subsequent heavy ion irradiation," *Nanotechnology* **31**, 455706 (2020).

[28]C. Hubert, L. Billot, P. M. Adam, R. Bachelot, P. Royer, J. Grand, D. Gindre, K. D. Dorkenoo, A. Fort, "Role of surface plasmon in second harmonic generation from gold nanorods," *Appl. Phys. Lett.* **90**, 181105 (2007).

[29]C. Janisch, Y. Wang, D. Ma, N. Mehta, A. L. Elias, N. Perea-Lopez, M. Terrones, V. Crespi, Z. Liu, "Extraordinary Second Harmonic Generation in Tungsten Disulfide Monolayers," *Sci. Rep.* **4**, 5530 (2014).

[30]N. Kumar, S. Najmaei, Q. N. Cui, F. Ceballos, P. M. Ajayan, J. Lou, H. Zhao, "Second harmonic microscopy of monolayer MoS_2," *Phys. Rev. B* **87**, 161403 (2013).

[31]X. Yin, Z. Ye, D. A. Chenet, Y. Ye, K. O'Brien, J. C. Hone, X. Zhang, "Edge Nonlinear Optics on a MoS_2 Atomic Monolayer," *Science* **344**, 488-490 (2014).

[32]J. Du, J. Shi, C. Li, Q. Shang, X. Liu, Y. Huang, Q. Zhang, "An on-Si directional second harmonic generation amplifier for MoS_2/WS_2 heterostructure," *Nano Res* **16**, 4061-4066 (2023).

[33]X. BAO, X. ZENG, J. SHI, W. ZHANG, X. Liu, "Manipulation of the second harmonic generation in two-dimensional transition metal dichalcogenides via micro-nano structures," *Sci. Sin.-Phys. Mech. Astron.* **53**, 284206 (2023).

[34]J. Shi, X. Wu, K. Wu, S. Zhang, X. Sui, W. Du, S. Yue, Y. Liang, C. Jiang, Z. Wang, W. Wang, L. Liu, B. Wu, Q. Zhang, Y. Huang, C.-W. Qiu, X. Liu, "Giant Enhancement and Directional Second Harmonic Emission from Monolayer WS_2 on Silicon Substrate via Fabry-Pérot Micro-Cavity," *ACS Nano* **16**, 13933-13941 (2022).

[35]C. Li, X. Lu, A. Srivastava, S. D. Storm, R. Gelfand, M. Pelton, M. Sukharev, H. Harutyunyan, "Second Harmonic Generation from a Single Plasmonic Nanorod Strongly Coupled to a WSe_2 Monolayer," *Nano Lett.* **21**, 1599-1605 (2020).

[36]S. Zhu, R. Duan, X. Xu, F. Sun, W. Chen, F. Wang, S. Li, M. Ye, X. Zhou, J. Cheng, Y. Wu, H. Liang, J. Kono, X. Li, Z. Liu, Q. J. Wang, "Strong nonlinear optical processes with extraordinary polarization anisotropy in inversion-symmetry broken two-dimensional PdPSe," *Light-Sci. Appl.* **13**, 119 (2024).

[37]M. A. Weissflog, A. Fedotova, Y. Tang, E. A. Santos, B. Laudert, S. Shinde, F. Abtahi, M. Afsharnia, I. Pérez Pérez, S. Ritter, H. Qin, J. Janousek, S. Shradha, I. Staude, S. Saravi, T. Pertsch, F. Setzpfandt, Y. Lu, F. Eilenberger, "A tunable transition metal dichalcogenide entangled photon-pair source," *Nat. Commun.* **15**, 7600 (2024).